Food Chemistry 404 (2023) 134580

Contents lists available at ScienceDirect

Food Chemistry

journal homepage: www.elsevier.com/locate/foodchem

Elucidating the inhibitory mechanism on polyphenol oxidase from mushroom and melanosis formation by slightly acid electrolysed water

Yun He [a,b], Isaac Kang Xing Yeo [a,b], Chenxi Guo [a,b], Yi Kai [a,b], Yuyun Lu [a], Hongshun Yang [a,b,*]

[a] Department of Food Science and Technology, National University of Singapore, Science Drive 2, Singapore 117542, Singapore
[b] National University of Singapore (Suzhou) Research Institute, 377 Lin Quan Street, Suzhou Industrial Park, Suzhou, Jiangsu 215123, PR China

ARTICLE INFO

Keywords:
Melanosis
Polyphenol oxidase
Conformation change
Molecular docking
Dihydroxyphenylalanine (DOPA)
Enzymatic browning
Color

ABSTRACT

It has been revealed that slightly acid electrolysed water (SAEW) could delay enzymatic browning and melanin formation in food. In this work, multi-spectroscopic methods and UHPLC-Q-TOF-MS were combined to study the underlying reason. The reversible mixed-type inhibition mode of HOCl (main components in SAEW) was determined. The ground state complex formation quenched the intrinsic fluorescence of polyphenol oxidase (PPO) and it was stable at lower temperature. The PPO conformational change (transformation from α-helix to β-sheet) induced by SAEW was confirmed by 3D fluorescence and Circular dichroism (CD) spectrum. Moreover, the driving force of the interaction between HOCl and PPO was hydrogen bond, which was validated by the molecular docking result. Besides, the formation of melanin related compounds including dihydroxyphenylalanine (DOPA), dopaquinone, dopachrome, 5,6-dihydroxyindole-2-carboxylic acid (DHICA), 5,6-dihydroxyindole (DHI), and 5,6-indolequinone were significantly inhibited by SAEW treatment. These results demonstrated the potential of SAEW as a PPO inhibitor in the food industry.

1. Introduction

Polyphenol oxidase (PPO) is a commonly found enzyme presented in fruits, seafood, vegetables and microorganisms. The common part in all PPO is their binuclear type III copper centre containing two copper atoms each connected with six histidine molecules in their active site (Marusek, Trobaugh, Flurkey, & Inlow, 2006) It catalyses a series of reactions including the hydroxylation of monophenols to *o*-diphenols and the oxidation of *o*-diphenols to *o*-quinones (Goncalves & de Oliveira, 2016). The presentation of PPO poses a threat to the food industry including the browning of fruits and vegetables and black spot formation in shrimp, negatively affecting the sensory perception and nutritive value of these food products (Cheng et al., 2020; Sae-leaw & Benjakul, 2019).

Hence, PPO inhibitors have been explored to control the melanosis and extend the shelf life of food products. These agents were developed based on the main components crucial for the undesirable enzymatic reaction by eliminating the enzyme, oxygen or substrate (Nirmal, Benjakul, Ahmad, Arfat, & Panichayupakaranant, 2015). Polyphenols have been extensively studied for control of discolouration of crustaceans during storage (Sae-leaw & Benjakul, 2019; Sae-leaw, Benjakul, & Simpson, 2017). The melanosis of Pacific white shrimp (*Litopenaeus vannamei*) treated with pomegranate peel extract and ethanoic extracts from avocado seed and peel could be delayed. The mechanism of inhibition of melanosis formation may be due to the ability of some polyphenols to interact with or compete with the active site of the PPO because of their structural similarity to the substrate (Abbasvali, Ranaei, Shekarforoush, & Moshtaghi, 2016; Basiri, Shekarforoush, Aminlari, & Akbari, 2014). Nonetheless, Their use is limited by the low extraction rates (Sae-leaw & Benjakul, 2019). Besides, the possible polyphenol-protein interactions might lead to a detrimental effect on the *in vivo* bioavailability of shrimp protein as well as the unfavorable impact on sensory characteristics (Gomez-Guillen & Montero, 2007). More convenient and cost-effective methods need to be developed for the alleviation of melanosis formation of crustaceans during storage.

The effectiveness of slightly acid electrolysed water (SAEW) for colour conservation of food has been previously demonstrated (He et al., 2022; Jia, Shi, Song, & Li, 2015). The SAEW treatment with FAC value of 25 mg/L effectively reduced Chinese yam browning during storage. In our previous research, the shrimp was immersed in SAEW ice with FAC value of 30 mg/L for 7 days. And it was found that the melanosis formation and discolouration of shrimp was retarded by the SAEW ice

* Corresponding author at: Department of Food Science and Technology, National University of Singapore, Singapore 117542, Singapore.
E-mail address: fstynghs@nus.edu.sg (H. Yang).

https://doi.org/10.1016/j.foodchem.2022.134580
Received 3 June 2022; Received in revised form 13 September 2022; Accepted 8 October 2022
Available online 12 October 2022

during the whole storage period (He et al., 2022), The activity of PPO enzyme extracted from these food products was inhibited by SAEW during the whole storage period. However, the underlying mechanism on how the SAEW inhibited the PPO activity and how it regulated the formation of the melanosis remains unknown.

In this work, we aimed to elucidate the inhibition mechanism of SAEW on PPO activity and melanin formation progress. Specifically, the inhibition kinetics was conducted to elucidate the reversibility and inhibition type of SAEW on PPO. The fluorescence quenching spectroscopy was used to illustrate the binding and quenching constant, enthalpy and entropy alternation of interactions. Circular dichroism (CD) spectroscopy clarified the conformation changes of PPO induced by SAEW. Molecular docking was applied to verify the potential interaction between SAEW and PPO were simulated by. Moreover, the products of the PPO catalysed reaction in absence and presence of SAEW were identified and quantified using ultra-high performance liquid chromatography-quadrupole time-of-flight mass spectrometry (UHPLC-Q-TOF-MS). This study emphasised on the mechanism involving PPO and SAEW, also gave valid information for usage of SAEW as PPO inhibitor in food industry.

2. Materials and methods

2.1. Preparation of reagents solution

The SAEW was generated according to the method described by He, Zhao, Chen, Zhao, and Yang (2021) by electrolysis of 1 % (w/v) NaCl solution combined with 4 mmol/L $NaHCO_3$ (Sigma-Aldrich, St Louis, MO, USA). Free available chlorine (FAC), pH, and oxidation- reduction potential (ORP) were tested by a chorine test kit (Merck Pte, ltd, Singapore), a pH meter (Thermo Scientific, Waltham, MA, USA), and an ORP meter (Metrohm Singapore Pte, ltd, Singapore), respectively. The SAEW was prepared by dilution with deionised (DI) water to achieve final FAC concentrations of 1.0, 2.0, 3.0, 4.0 mg/Lfor following experiments. And the DI water was used as the control group. PPO from mushroom (EC 1.14.18.1, 100,000 U/mg, Sigma Aldrich, St. Louis, MO) was dissolved in phosphate buffer (50 mM, pH 6.5). L-3,4-dihydroxyphenylalanine (L-DOPA) substrate solutions were also made by diluting with PBS to achieve final concentrations of 0.5, 1.0, 1.5, 2.0, and 2.5 mM, respectively.

2.2. Inhibition kinetics analysis

PPO activity was conducted using L-DOPA as a substrate according to the method of (Nirmal & Benjakul, 2012) with several modifications. The SAEW was prepared by dilution with deionised (DI) water to achieve final FAC concentrations of 1.0, 2.0, 3.0, 4.0 mg/L. SAEW solution (15 μL) was added into 30 μL PPO solution, and then 140 μL of L-DOPA of each concentration was added to start the reaction. The absorbance readings were taken at 475 nm every 45 s using a UV–vis spectrophotometer (BioTek Synergy HTX, USA) to monitor formation of dopachrome. The inhibition type for SAEW was investigated by kinetic analysis. The plots of V against different PPO concentrations at different FAC levels of SAEW were conducted to investigate the reaction reversibility. In addition, the Lineweaver-Burk equation in double reciprocal form was used to elucidate the mechanism of mixed-type inhibition as follows:

$$\frac{1}{V}=\frac{K_m}{V_{\max}}\left(1+\frac{[I]}{K_i}\right)\frac{1}{[S]}+\frac{1}{V_{\max}}\left(1+\frac{[I]}{\alpha K_i}\right) \quad (1)$$

Second plots can be constructed from.

$$Slope = \frac{K_m}{V_{\max}}+\frac{K_m}{V_{\max}\ K_i}[I] \quad (2)$$

$$Y-intercept = \frac{1}{V_{\max}}+\frac{1}{V_{\max}\ (K_i)}\ [I] \quad (3)$$

where V represents the PPO reaction rate. K_i and K_m are the inhibition constant and Michaelis-Menten constant, respectively. [I] and [S] represents the concentrations of inhibitor and substrate, respectively. The secondary replots of slope or Y-intercept versus [I] is linearly fitted, indicating a single inhibition site or a single class of inhibition site.

2.3. Intrinsic fluorescence spectra measurement

Intrinsic fluorescence of different samples was measured using fluorescence spectrophotometer (Horiba, US). PPO solutions (1.0 mg/mL) was dissolved in phosphate buffer. Multiple samples of SAEW were diluted with deionised water to achieve final FAC concentrations of 1.0, 1.5, 2.0, 2.5, 3.0, and 4.0 mg/L at different temperatures (277, 298, and 308 K). The excitation wavelength was set to 280 nm, and the spectra was scanned from 300 nm to 500 nm. The excitation and emission slit widths were set at 5 nm, and the voltage was 1450 v. It was also possible to determine the nature of the quenching, be it dynamic or static quenching. The fluorescence quenching was analysed by the Stern-Volmer equation (Eq. (4)).

$$F_0/F = 1+K_q\tau_0[Q] = 1+K_{SV}[Q] \quad (4)$$

where F_0 and F represent the fluorescence intensity in the absence and presence of SAEW, respectively. τ0 (10^{-8} s) is the average lifetime of unquenched fluorophore. [Q] is the concentration of the quencher (in this case SAEW). The bimolecular quenching rate constant (K_q) and the Stern-Volmer quenching constant (K_{sv}) could be calculated for the slop of the plot.

For static quenching, a modified Stern-Volmer equation using double logarithms was introduced (Eq. (5)).

$$\log[(F_0-F)/F] = \log K_a + n\log[Q] \quad (5)$$

where K_a is the binding constant, and n is the number of binding sites.

The thermodynamic parameters for PPO and SAEW binding could be estimated by the Van't Hoff equation (Eq. (6)).

$$\ln K_a = -\frac{\Delta H}{RT}+\frac{\Delta S}{R} \quad (6)$$

where R is the gas constant, T is thermodynamic temperature.

Gibbs free energy (ΔG) of the quenching progress at different temperatures was calculated by Eq. (7).

$$\Delta G = \Delta H - T\Delta S \quad (7)$$

2.4. Three-dimensional fluorescence spectra measurement

Three-dimensional fluorescence spectra of PPO (1.0 mg/mL) in the absence and presence of SAEW with 2 mg/L FAC level was performed. the excitation wavelength was recorded between 200 nm and 320 nm with an increment of 2 nm, the emission wavelength was scanned from 220 nm to 500 nm with an increment of 2 nm, and the scan speed was set at 2400 nm/min. The excitation slit and emission slit were both 5 nm.

2.5. Secondary structure of PPO measurement using CD spectroscopy

The effect of SAEW on the secondary structure of PPO was measure by a CD spectrometer (J-1500, Jasco Corp., Japan). SAEW with FAC level of 0, 2, and 4 mg/L was mixed with 0.1 mg/mL PPO and detected at a wavelength range from 190 nm to 250 nm. BeStSel server (https://bestsel.elte.hu) was used to analyse the secondary structure elements (Micsonai et al., 2018).

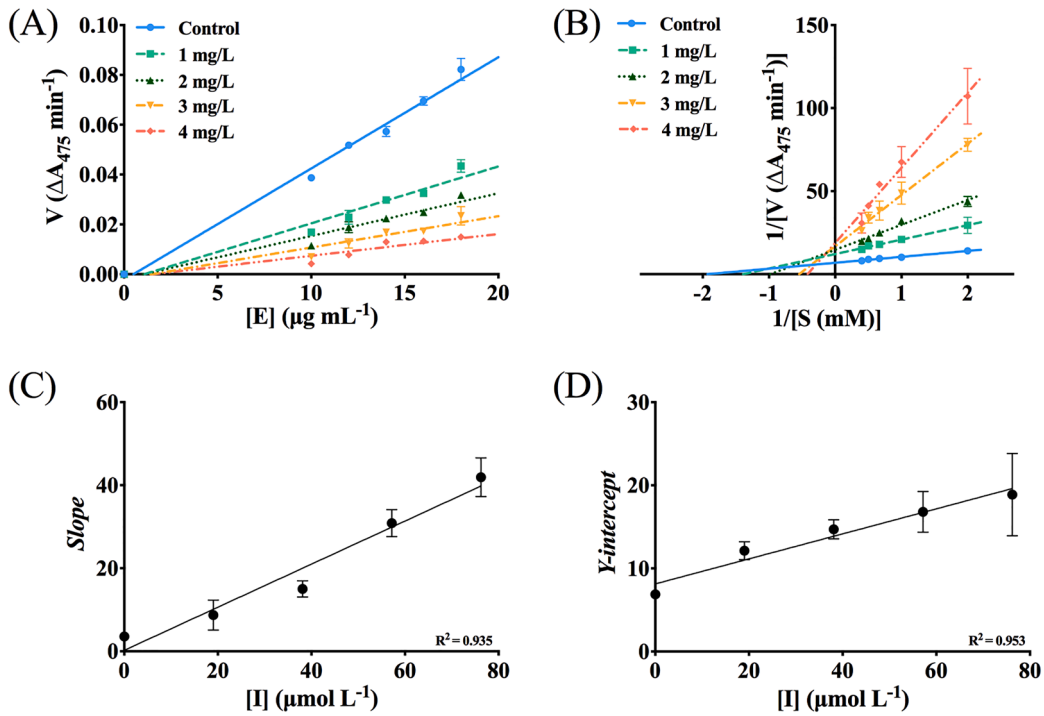

Fig. 1. Effect of SAEW on PPO activity. Plots of V versus [PPO] for SAEW at different FAC levels (A), Lineweaver-Buck plots for SAEW(B), the secondary replots of slope versus [SAEW] (C), and Y-intercept versus [SAEW] (D). Note: SAEW, slightly acid electrolysed water; PPO, polyphenol oxidase.

2.6. Molecular docking of PPO and SAEW

The computational molecular docking was applied to investigate the potential bind between PPO and HOCl using AutoDock Vina 1.2.3 according to the previous method (Cheng et al., 2020). The PPO structure was obtained from the RCSB Protein Data Bank (PDB ID: 2Y9W). The three-dimensional structure of HOCl was drawn by Chem3D Ultra 12.0 and the energy was minimised by MM2. Docking data with the lowest docking affinity was considered to be the most appropriate result and chosen for further analysis. The docking results were visualised and generated from PyMol 2.3.

2.7. Identification and quantification of PPO-catalysed reaction compounds

Tyrosine was chosen as the substrate for the PPO-catalysed reaction as the melanin formation in shrimp were reported to be related to tyrosine. PPO (100 U/mL) was mixed with SAEW with FAC level of 2 mg/L, HOCl solution (2 mg/L), and DI water, respectively. And tyrosine dissolved in phosphate buffer (2.5 mM) was added to start the reaction. The mixture was incubated for 10 min at room temperature. The PPO enzyme was further removed by ultrafiltration with vivaspin (molecular weight cutoff: 30 k) to stop the reaction (Inukai, Hara, & Ichinose, 2022). The formation of the reaction products was monitored using the ACQUITY UPLCTM I-Class PLUS system (Waters, Milford, MA) with a VION ion mobility spectroscopy quadrupole time-of-flight mass spectrometer (IMS-QTOF-MS) (Waters, Manchester, U.K.). ACQUITY UPLCr BEH C18 analytical column (2.1 × 100 mm^2, 1.7 μm) (Waters, Milford, MA) was used for analysis. The gradient elution was conducted using mobile phase consisted of 0.1 % (v/v) formic acid (FA) in water (A) and acetonitrile (ACN) (B) at a flow rate of 0.3 mL/min^{-1}. The gradient conditions were set as follows: 0–1 min 1 % B, 1–2.5 min 1–25 % B, 2.5–5.5 min: 25–32 % B, 5.5–14.5 min 32–100 % B, 14.5–16.5 min 100 % B, 16.5–17.0 min 100–1 % B, and 17–20 min 1 % B.

The capillary voltage was set at 2.2 kV for positive mode and 2.0 kV for negative mode. The source temperature was set to 120 °C and the desolvation nitrogen gas was adjusted to 500 °C with a flow rate of 600 L/h. The MS^E experiment simultaneously acquired in the *m/z* range of 50–1200 Da. A low-energy function (collision energy of 9.6 eV) and a high-energy function with collision energy varying linearly from 24 to 72 eV were developed. The Leucine enkephalin solution (100 ppb) in ACN/H_2O (50:50, v/v) containing 0.1 % FA was injected through a lockspray needle at a rate of 10 μL/min and collected every 5 min with a scan time of 0.3 s for automated mass measurements. The protonated and deprotonated molecules of leucine enkephalin (*m/z* 556.27658 in ESI^+ mode and *m/z* 554.26202 in ESI^- mode) were used for mass corrections, respectively, to confirm that mass measurements were accurate during the run. The UPLC-MS spectra were further analysed using the Progenesis QI software (V.2.4, Nonlinear Dynamics, Waters, Newcastle, U.K.). For compounds identification, the adducts $[M+H]^+$, $[M+NH_4]^+$, $[M+Na]^+$ and $[M+K]^+$ were chosen for the positive mode, and $[M-H]^-$ and $[M-H_2O-H]^-$ were applied for the negative mode. The significantly altered compounds in the reactions in the presence and absence of SAEW (VIP > 1, *P* value < 0.05 and CV ≤ 30) were carefully chosen for further analysis.

2.8. Data analysis

Analysis of variance (ANOVA) was conducted, and mean comparisons were made by Duncan's multiple range tests using SPSS Statistics 20 software (IBM Co., USA). The significant differences between means with groups were set at $P < 0.05$.

3. Results and discussion

3.1. Reversibility and inhibition type analysis of SAEW on PPO

To determine the mode of inhibition of L-DOPA oxidation by SAEW, the kinetics of inhibition following the Michaelis Menten equation were investigated. The plots of PPO activity (V) versus SAEW at different FAC concentrations were constructed to elucidate the reversibility of inhibition of SAEW on PPO. As shown in Fig. 1A, good linearity was

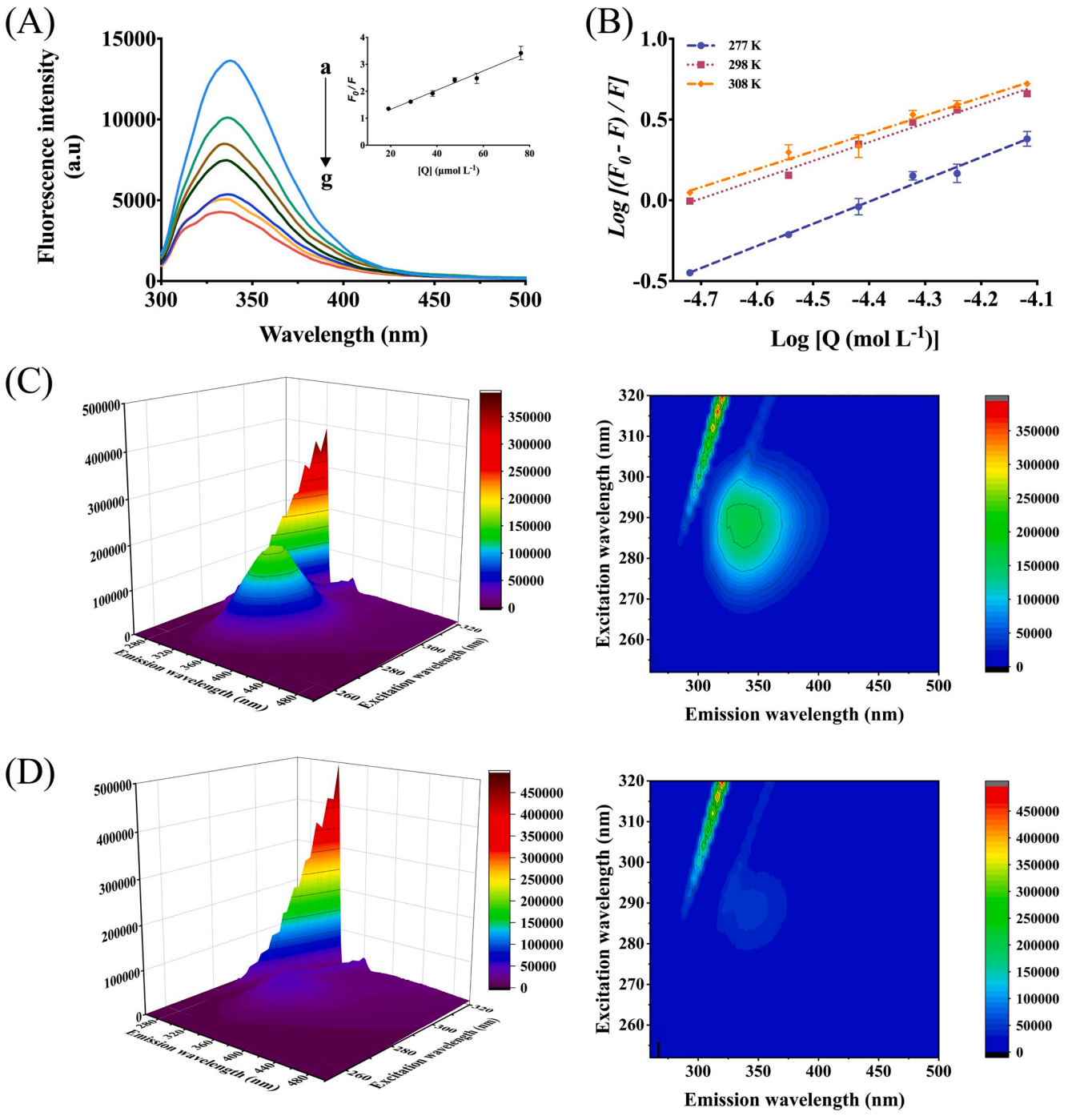

Fig. 2. Fluorescence emission spectra of PPO in the presence of 0–4 mg/L FAC level of SAEW at 277 K. FAC level of SAEW 0, 1, 1.5, 2, 2.5, 3, and 4 mg/L curves a → g, respectively (A). The inset showed the Stern-Volmer plot for the quenching of PPO by SAEW at 277 K. The double-logarithmic regression plots of PPO treated with SAEW at 277 K, 298 K and 308 K (B). Three-dimensional (3D) fluorescence spectra of PPO in the absence (C) and presence (D) of SAEW. Note: SAEW, slightly acid electrolysed water; PPO, polyphenol oxidase.

observed for all plots and these lines all passed almost through the origin. Moreover, the slope of the curve decreased with the increasing FAC concentration of SAEW. These results demonstrated that SAEW reversibly inhibited PPO activity, and noncovalent bond was formed during the interaction of SAEW and PPO. Similar results were also observed in the inhibition of gentisic acid and chlorogenic acid on PPO (Cheng et al., 2020; Zhou, Xiong, Liu, & Zou, 2017).

The Lineweaver–Buck double reciprocal plot was further introduced to investigate the inhibition type of SAEW on PPO according to previous report (Hu et al., 2012). As can be seen from Fig. 1B, both the X axis intercept ($1/V_{max}$) and Y axis intercept ($-1/K_m$) changed with the different FAC level of SAEW, suggesting that SAEW induced a mixed-type inhibition on PPO in which the inhibitor bound both the free enzyme and the enzyme-substrate (ES) complex. Moreover, the increasing FAC level of SAEW further lead to the decrease of V_{max} and increase of K_m, indicating that SAEW reduced the overall affinity of PPO for its substrate L-DOPA and more favorably bound to free enzyme, rather than to ES complex (Ramsay & Tipton, 2017). Similar observation was made by (Cheng et al., 2020) about the nature of chlorogenic acid as mixed mode inhibitor. Interestingly, the slope and Y-intercept of the

Table 1
The fitting parameters of Stern-Volmer models and the quenching constants for SAEW and PPO at different temperatures.

T (K)	R^2	RMSE ($\times 10^{-2}$)	K_q ($\times 10^{12}$ L/mol s^{-1})	K_{sv} ($\times 10^4$ L/mol)
277	0.94	7.4	3.66 ± 0.14a	3.66 ± 0.14a
298	0.98	10.3	6.34 ± 0.69b	6.34 ± 0.69b
308	0.97	13.1	7.26 ± 0.47b	7.26 ± 0.47b

Note: within the same column, values with different lowercase letters are significantly different ($P < 0.05$). Note: SAEW, slightly acid electrolysed water; PPO, polyphenol oxidase.

Table 2
The fitting parameters of double-logarithmic models, the binding constants, and thermodynamic parameters for the interaction of SAEW with PPO at different temperatures.

T (K)	R^2	RMSE ($\times 10^{-2}$)	Kα ($\times 10^5$ L/mol)	N	ΔG (KJ mol^{-1})	ΔH (KJ mol^{-1})	ΔS (J mol^{-1} K^{-1})
277	0.97	2.1	10.77 ± 2.45b	1.37 ± 0.03a	−31.93 ± 0.68a	−38.84 ± 3.43	−24.95 ± 9.99
298	0.99	2.0	3.18 ± 1.21a	1.17 ± 0.04a	−31.40 ± 0.46a		
308	0.96	2.5	1.98 ± 0.01a	1.11 ± 0.01a	−31.15 ± 0.36a		

Note: within the same column, values with different lowercase letters are significantly different ($P < 0.05$). Note: SAEW, slightly acid electrolysed water; PPO, polyphenol oxidase.

Lineweaver-Burk plot against the corresponding HOCl concertation were then plotted and both yielded first order curves (Fig. 1C-D), demonstrating that SAEW exhibited a class of inhibitory sites or a single inhibitory site on PPO (Hemachandran et al., 2017).

3.2. The fluorescence quenching mechanism analysis

The protein–ligand interaction is commonly investigated and identified by fluorescence quenching study, which could further help to study the mechanism in-depth (Ren, Xiong, Li, & Li, 2019). The intrinsic fluorescence of PPO was due to the presence of fluorophores tryptophan and tyrosine residues when excited at 280 m. As shown in Fig. 2A, the maximum peak position of PPO in the absence of SAEW was exhibited at 338 nm. After exposing to different FAC concentrations of SAEW, the peak florescence intensity decreased. The SAEW induced a concentration-dependent quenching of the the intrinsic fluorescence of PPO, suggesting the interactions between SAEW and fluorophores of PPO. Moreover, the emission wavelength at which the peak florescence was observed also shifted, from 338 nm for control sample to 316 nm for the samples 4 mg/L SAEW. The blue shifts of SAEW treated PPO protein could be explained by more burying of Trp residues inside the protein, as buried Trp induced blue shifts (Iqbal et al., 2020).

The quenching mechanism was further elucidated using Stern-Volmer equation (4). As depicted in Fig. 2A and Table 1, the plot of F_0/F of PPO versus the concentration of SAEW was linearly fitted with the high R^2 and low RMSE values at different temperatures (Ran, Yang, Chen, & Yang, 2022). The K_{sv} values were obtained from the slopes of the plot, while the K_q values were further calculated based on K_{sv}. K_q values at different temperature were all much greater than the maximum diffusion-limited quenching constant in water (2×10^{10} L/mol S^{-1}), revealing that the static quenching predominated in the interaction between SAEW and PPO, rather than dynamic quenching which was induced by collision (Yang, Xu, Liu, Yuan, & Gao, 2014). Static quenching was caused by the formation of the ground state complex. And the increasing of the temperature led to the rise in temperature K_q values (from 3.66×10^{12} at 277 K to 7.26×10^{12} L/mol s^{-1} at 308 K), The results was consistent with previous reports demonstration that the complex for static quenching became unstable at higher temperature and led to an increase in the quenching constant (Hemachandran et al., 2017; Liao et al., 2021).

For static quenching mechanism, a double-logarithmic equation (Eq. (5)) was applied to determine the binding constant (K_α) and number of binding sites (N), and the obtained data were shown in Fig. 2B and Table 2. The high R^2 and low RMSE values indicated the good linearity of the plots (Ran et al., 2022). And the K_α and N were further determined by the intercept and slope of the plots of $\log[(F_0\text{-}F)/F]$ versus $\log[Q]$, respectively. When the temperature increased from 277 to 298 K, the Kα value significantly decreased, indicating the complexes were stable at relative low temperature, revealing their interactions to exothermic reactions (Jia, Gao, Hao, & Tang, 2017). Moreover, the N values at different temperatures were almost equal to 1, indicating that single site in PPO was available for SAEW binding, which was corresponding well with previous inhibition kinetics result.

In general, the relative magnitude of the thermodynamic parameters can be used to determine the intermolecular interaction forces. The molecular structure of PPO did not change significantly at the three experimental temperatures (277, 298 and 308 K). The enthalpy change (ΔH) could be considered as a constant (Guan, Yan, Zhao, Sun, & Peng, 2018). The obtained K_α could be further applied to calculate the enthalpy change (ΔH), entropy change (ΔS) and Gibbs free energy change (ΔG) using Eqs. (6) and (7) as shown in Table 2. Previous studies have shown that hydrophobic interactions were the main driving force when $\Delta H > 0$ and $\Delta S > 0$. Van der Waals forces and hydrogen bonds played a vital role when $\Delta H < 0$ and $\Delta S < 0$. When $\Delta H \approx 0$ and $\Delta S > 0$, the electrostatic forces were mainly formed (Cheng et al., 2020). In our study, the negative value of ΔG represented that the binding between PPO and SAEW was spontaneous at the corresponding temperature. ΔH and ΔS were both smaller than 0, suggesting Van der Waals forces and hydrogen bonds were mainly formed during interaction (He, Xu, Zeng, Qin, & Chen, 2015).

The effect of SAEW addition on detailed conformational information of PPO was monitored by 3D fluorescence spectroscopy. The 3D spectra were depicted in Fig. 2C-D. Strong fluorescence peak appears at the excitation wavelength at around 280 nm, due to the fluorescent amino acid residues. Upon interaction with SAEW, a decrement of peak intensity was induced, depicting conformational changes. These results were in line with the intrinsic fluorescence results.

3.3. PPO secondary structure analysis

The CD spectroscopy has been widely used to analysis the secondary structure, unfolding of protein when binding with other compounds (Akita et al., 2020; Li, Bai, Ji, & Jin, 2020). As can be seen from Fig. 3A, the negative ellipticities at 208 and 222 nm is attributed to the peaks of α-helix structure of PPO. And the α-helix was shown to be the main structure of PPO, which was consistent with previous research (Liao et al., 2021). After treatment with SAEW, significant raise in the ellipticity of PPO at 208 nm was observed, and it gradually increased with the increasing FAC level of SAEW, indicating the decrease of ordered structure of PPO. However, there is no significant change in peak shape or position, indicating that the α-helix remained dominant.

The main components of the secondary structure were further calculated to better elucidate the effect of SAEW treatment on the secondary structure. The α-helix content decreased from 25.5 % to 21.8 %, while the level of β-sheet increased from 13.0 % to 23.5 %, while there was no obvious change in β-turn and random coil, demonstrating that SAEW could induce the conversion of the α-helix to a β-sheet when binding to PPO molecules. The natural PPO has been reported to consist of a mostly α-helical structure, with the catalytically essential dinuclear copper-binding site located at the centre of two pairs of anti-parallel α-helix (Ismaya et al., 2011). Similar transformation from α-helix to

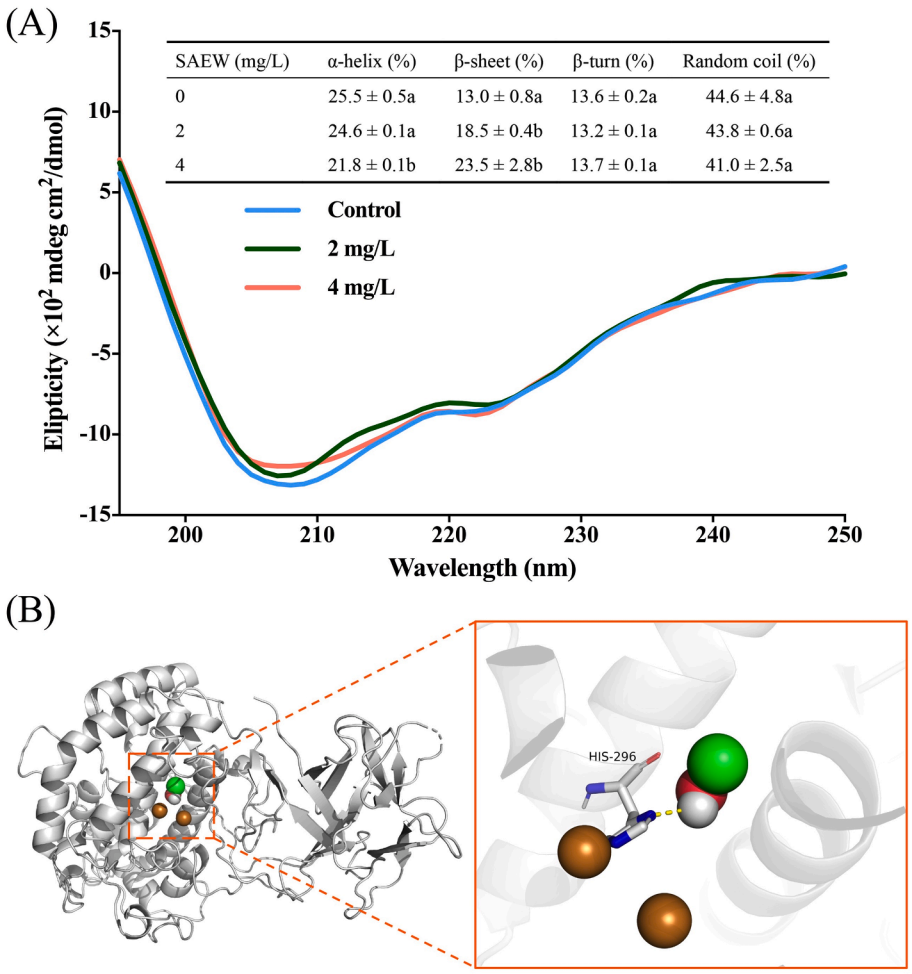

Fig. 3. CD spectra of SAEW-treated PPO. The inset showed the secondary structure content calculated from CD spectra of SAEW-treated PPO (A). The interactions between SAEW and PPO simulated by AutoDock Vina with the lowest docking affinity. PPO is shown in the animated form. The detailed view showed the adjacent residue of the binding site of SAEW and PPO (B). Note: The atoms of SAEW are colour-coded as follows: H, grey; O, red. Cl, green. The two yellow atoms represented the Cu ions in active site of PPO. Note: SAEW, slightly acid electrolysed water; PPO, polyphenol oxidase. (For interpretation of the references to color in this figure legend, the reader is referred to the web version of this article.)

β-sheet has been found in salicylic acid-treated PPO (Liao et al., 2021) and ultrasound-treated PPO (Zhou et al., 2016), which was usually accompanied by lower PPO enzyme activity. This phenomenon could be explained by the disruption of the hydrogen bonding network that maintained the stability of the α-helical and β-folded structures in the PPO enzyme (Liao et al., 2021).

3.4. Computational simulation of SAEW on PPO

The interaction between HOCl and PPO was identified and verified using the molecular docking method. HOCl was used because it was the main chlorine form presented in the SAEW at the pH used in our study (Rahman, Khan, & Oh, 2016). The molecular docking result with the lowest binding affinity is shown in Fig. 3B. The catalytic core of PPO was like a pocket, consisting of two Cu ions and six histidine residues, including His 61, His 85, His 94, His 259, His 263 and His 296 (Ismaya et al., 2011). And the HOCl was found to interact with the His 296 of PPO via hydrogen bond with binding energy of − 2.3 kcal/mol, indicating that the binding site was located in the catalytic active site of PPO, further avoiding the entry of substrate. Besides, the docking results provided the verification of the thermodynamic parameters based on the fluorescence results, demonstrating that the main drive force between SAEW and PPO was hydrogen bond. The modelling results combined with enzyme conformation analysis suggested that HOCl could interact well with the primary amino acid residues on the active site of PPO. And it could be deduced that the insertion of HOCl into the active site of PPO and the disrupted structure of the PPO might avoid the entrance of the substrate, resulting in the decrease of PPO activity ultimately.

3.5. Comparison of PPO catalysed reaction compounds

To further understand the effect of SAEW on regulating the melanin formation, the tyrosine was chosen as substrate and the PPO catalysed compounds in the absence and presence of SAEW were identified and quantified. Besides, the control experiment using HOCl in place of SAEW has been performed to verify the effect of this main component of SAEW on the melanin formation. In our study, many of the reported melanin-forming intermediates were potentially identified including DOPA, dopaquinone, dopachrome, 5,6-dihydroxyindole-2-carboxylic acid (DHICA), 5,6-dihydroxyindole (DHI), and 5,6-indolequinone shown in Fig. S1 and Table S1. Relatively high scores and fragmentation scores of these compounds was obtained indicating the high confidence of these compounds (Arndt, Wachsmuth, Buchholz, & Bentley, 2020). Their fold change comparison between these groups was further conducted. Based on the putative compounds and previous research, the schematic synthesis of PPO catalysed melanin was given and shown in Fig. 4. the oxidation of tyrosine was catalysed by PPO to form dopaquinone, which underwent rapid intramolecular cyclization and converted to cyclodopa (Bronze-Uhle et al., 2013). Dopachrome and DOPA were then produced by a spontaneous redox reaction between cyclodopa and uncycled dopaquinone. The generated DOPA could be further oxidised to dopaquinone. Dopachrome was considered as an important intermediate during melanosis formation which could evolve into dihydroxyindole with putative decarboxylation. Therefore, non-enzymatic transformation may occur mainly to produce DHI and, to a lesser extent, DHICA (Edge et al., 2006; Sugumaran, Evans, Ito, & Wakamatsu, 2020). Further oxidative polymerisation of DHICA and DHI produced

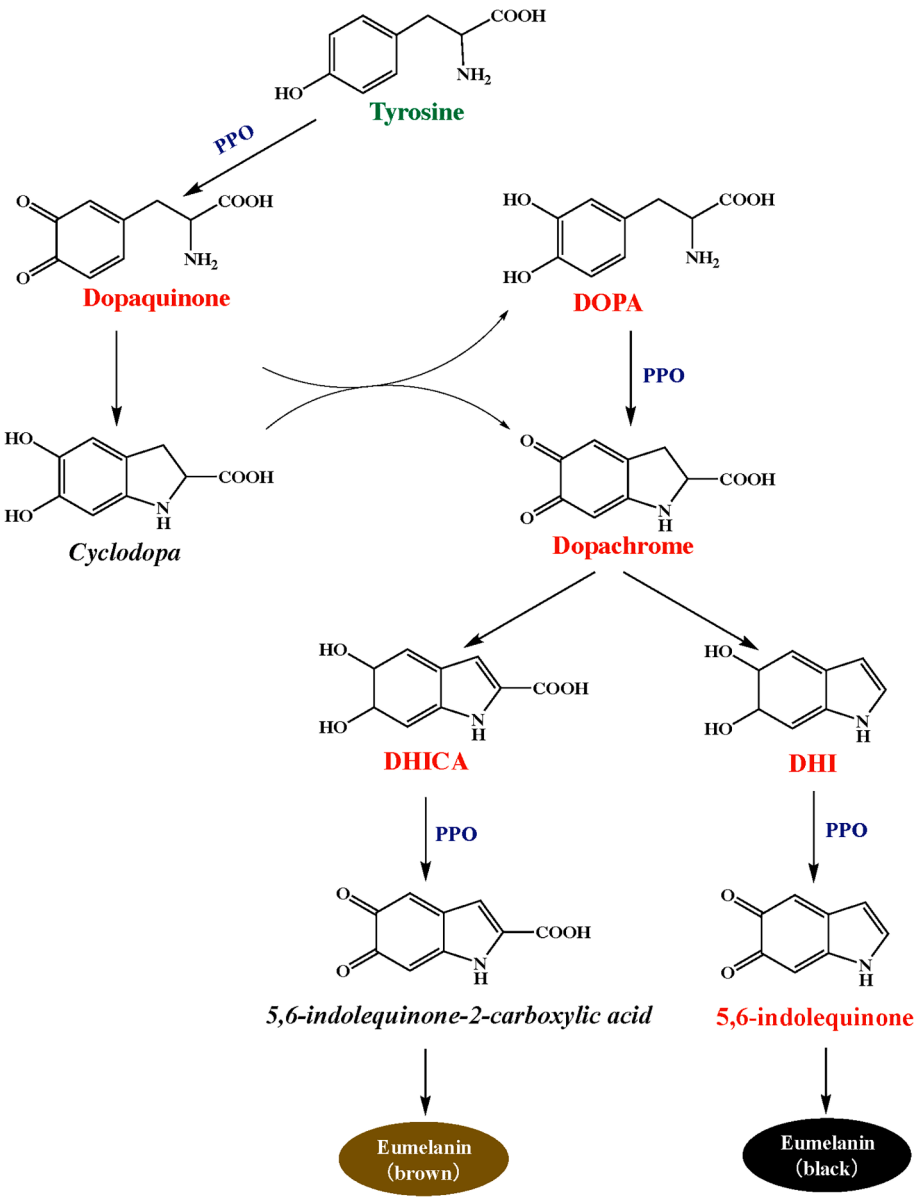

Fig. 4. The schematic synthesis of PPO catalysed melanin based on the potential compounds identified in UPLC-MS and proposed mechanism of SAEW regulation on melanin formation. Note: Compounds coloured in green or red represented significantly higher and lower concentration in SAEW group as compared to control group, respectively; compounds in italic black were not identified. Note: SAEW, slightly acid electrolysed water; PPO, polyphenol oxidase Several steps were referred to Swarup and Jong-Whan (2021) and Edge et al. (2006). (For interpretation of the references to color in this figure legend, the reader is referred to the web version of this article.)

eumelanin, which appeared brown and black, respectively (Swarup & Jong-Whan, 2021).

Interestingly, in the presence of SAEW, almost all the identified reaction products exhibited a significant decreasing trend, while the tyrosine consumption is relatively low in the SAEW and HOCl group when compared to the DI treated group. Similar patterns in regulating the reaction progress were observed in the SAEW group and HOCl group, demonstrating that HOCl played a vital role in regulating the melanin production. The inhibition of these compounds formation could be attributed to several reasons. Firstly, the PPO activity was inhibited by SAEW treatment. While in the process of melanin formation, PPO catalysed several reactive processes including monophenols hydroxylation to form o-diphenols and oxidation of o-diphenols to form o-quinones, i.e., it was directly involved in the formation of dopaquinone, dopachrome, and 5,6-indolequinone (Sabarre & Yagonia-Lobarbio, 2022). Therefore, lower levels of these compounds were observed. The gradual reaction further lead to the depleted level of DOPA, DHICA, and DHI. Meanwhile, although the compounds were not identified in our study, the reaction of HOCl with tyrosine, DOPA and dopaquinone, respectively, might occur according to previous report, further blocking the next reactions and thus inhibiting melanin formation (Chen, Wang, Zhou, & Huang, 2011; de Bruin-Hoegee et al., 2022). These results explained the regulatory mechanism of SAEW in the specific melanin formation reaction. And it provided some theoretical basis for the inhibition of enzymatic browning and the production of melanin by SAEW (He et al., 2022; Jia et al., 2015). However, PPO from various food species exhibited different isoforms with varying molecular weight (MW) and kinetic parameter (Sae-leaw & Benjakul, 2019). Further investigation is needed to understand the inhibition mechanism of SAEW involved in the *in vivo* melanosis formation progress. A better comprehension regarding *in vivo* mechanism can provide more technical guidance for the practical application of colour conservation in food industry.

4. Conclusions

In this study, the underlying mechanism by which SAEW inhibit melanin formation was elucidated by multi-spectroscopic and MS method. The inhibition kinetic analysis revealed that PPO reversibly bound to HOCl (main components presented in SAEW) via the mixed-

type mode, reducing its affinity for substrate. The fluorescence data demonstrated that the binding interactions of SAEW with HOCl were spontaneous processes mostly driven by hydrogen bond, which was verified by the molecular docking results. Meanwhile, the interaction between HOCl and PPO led to the conformational changes of PPO, from α-helix to β-sheet. Computational docking simulation predicted that HOCl inserted into PPO and interact with amino acid residue located within the active site pocket with a binding energy of −2.3 kcal/mol to inhibit the PPO activity by avoiding the entry of the substrate. Moreover, the formation of melanosis related compounds including dopaquionone, DOPA, dopachrome, DHICA, DHI and 5,6-indolequinone, which was directly or indirectly involved in PPO catalysed reaction, was inhibited by SAEW addition. These results have provided a deeper insight of melanin inhibition by SAEW and further demonstrate the potential of SAEW for food preservation applications.

CRediT authorship contribution statement

Yun He: Data curation, Formal analysis, Investigation, Methodology, Resources, Software, Validation, Visualization, Writing – original draft. **Isaac Kang Xing Yeo:** Data curation, Formal analysis, Investigation. **Chenxi Guo:** Resources, Software. **Yi Kai:** Investigation, Methodology. **Yuyun Lu:** Methodology, Resources, Software. **Hongshun Yang:** Conceptualization, Funding acquisition, Project administration, Supervision, Writing – review & editing.

Declaration of Competing Interest

The authors declare that they have no known competing financial interests or personal relationships that could have appeared to influence the work reported in this paper.

Data availability

Data will be made available on request.

Acknowledgments

This work was funded by Singapore Ministry of Education Academic Research Fund Tier 1 (A-8000469-00-00), and an industry grant supported by Changzhou Qihui Management & Consulting Co., Ltd (R-160-000-A82-597).

Appendix A. Supplementary data

Supplementary data to this article can be found online at https://doi.org/10.1016/j.foodchem.2022.134580.

References

Abbasvali, M., Ranaei, A., Shekarforoush, S. S., & Moshtaghi, H. (2016). The effects of aqueous and alcoholic Saffron (*Crocus sativus*) tepal extracts on quality and shelf-life of Pacific white shrimp (*Litopeneous vannamei*) during iced storage. *Journal of Food Quality, 39*(6), 732–742.

Akita, M., Nishikawa, Y., Shigenobu, Y., Ambe, D., Morita, T., Morioka, K., & Adachi, K. (2020). Correlation of proline, hydroxyproline and serine content, denaturation temperature and circular dichroism analysis of type I collagen with the physiological temperature of marine teleosts. *Food Chemistry, 329*, Article 126775.

Arndt, D., Wachsmuth, C., Buchholz, C., & Bentley, M. (2020). A complex matrix characterization approach, applied to cigarette smoke, that integrates multiple analytical methods and compound identification strategies for non-targeted liquid chromatography with high-resolution mass spectrometry. *Rapid Communications in Mass Spectrometry, 34*(2), e8571.

Basiri, S., Shekarforoush, S. S., Aminlari, M., & Akbari, S. (2014). The effect of pomegranate peel extract (PPE) on the polyphenol oxidase (PPO) and quality of Pacific white shrimp (*Litopenaeus vannamei*) during refrigerated storage. *LWT - Food Science and Technology, 60*, 1025–1033.

Bronze-Uhle, E. S., Batagin-Neto, A., Xavier, P. H. P., Fernandes, N. I., de Azevedo, E. R., & Graeff, C. F. O. (2013). Synthesis and characterization of melanin in DMSO. *Journal of Molecular Structure, 1047*, 102–108.

Chen, S. K., Wang, B. C., Zhou, T. G., & Huang, W. Z. (2011). Theoretical study of the adsorption of DOPA-quinone and DOPA-quinone chlorides on Cu (100) surface. *Applied Surface Science, 257*, 7938–7943.

Cheng, D., Wang, G., Tang, J., Yao, C., Li, P., Song, Q., & Wang, C. (2020). Inhibitory effect of chlorogenic acid on polyphenol oxidase and browning of fresh-cut potatoes. *Postharvest Biology and Technology, 168*, Article 111282.

de Bruin-Hoegee, M., van Damme, I. M., van Groningen, T., van der Riet-van Oeveren, D., Noort, D., & van Astem, A. C. (2022). Elucidation of *in Vitro* chlorinated tyrosine adducts in blood plasma as selective biomarkers of chlorine exposure. *Chemical Research in Toxicology*, 1–10.

Edge, R., dIschia, M., Land, E. J., Napolitano, A., Navaratnam, S., Panzella, L., Pezzella, A., Ramsden, C. A., & Riley, P. A. (2006). Dopaquinone redox exchange with dihydroxyindole and dihydroxyindole carboxylic acid. *Pigment Cell Research, 19*, 443–450.

Gomez-Guillen, M. C., & Montero, M. P. (2007). Polyphenol uses in seafood conservation. *American Journal of Food Technology, 2*(7), 593–601.

Goncalves, A. A., & de Oliveira, A. R. M. (2016). Melanosis in crustaceans: A review. *LWT-Food Science and Technology, 65*, 791–799.

Guan, J., Yan, X., Zhao, Y., Sun, Y., & Peng, X. (2018). Binding studies of triclocarban with bovine serum albumin: Insights from multi-spectroscopy and molecular modeling methods. *Spectrochimica Acta Part A: Molecular and Biomolecular Spectroscopy, 202*, 1–12.

He, Y., Xie, Z., Xu, Y., Zhao, X., Zhao, L., & Yang, H. (2022). Preservative effect of slightly acid electrolysed water ice generated by the developed sanitising unit on shrimp (*Penaeus vannamei*). *Food Control, 136*, Article 108876.

He, Z., Xu, M., Zeng, M., Qin, F., & Chen, J. (2015). Interactions of milk α- and β-casein with malvidin-3-O-glucoside and their effects on the stability of grape skin anthocyanin extracts. *Food Chemistry, 199*, 314–322.

He, Y., Zhao, X., Chen, L., Zhao, L., & Yang, H. (2021). Effect of electrolysed water generated by sodium chloride combined with sodium bicarbonate solution against *Listeria innocua* in broth and on shrimp. *Food Control, 127*, Article 108134.

Hemachandran, H., Anantharaman, A., Mohan, S., Mohan, G., Kumar, D. T., Dey, D., … Ramamoorthy, S. (2017). Unraveling the inhibition mechanism of cyanidin-3-sophoroside on polyphenol oxidase and its effect on enzymatic browning of apples. *Food Chemistry, 227*, 102–110.

Hu, W. J., Yan, L., Park, D., Jeong, H. O., Chung, H. Y., Yang, J. M., … Qian, G. Y. (2012). Kinetic, structural and molecular docking studies on the inhibition of tyrosinase induced by arabinose. *International Journal of Biological Macromolecules, 50*(3), 694–700.

Inukai, S., Hara, S., & Ichinose, H. (2022). Tyrosine hydroxylase activity is regulated through the modification of the 176th cysteine residue. *Biochemical and Biophysical Research Communications, 589*, 209–214.

Iqbal, A., Murtaza, A., Marszałek, K., Iqbal, M. A., Chughtai, M. F. J., Hu, W., … Xu, X. Y. (2020). Inactivation and structural changes of polyphenol oxidase in quince (*Cydonia oblonga Miller*) juice subjected to ultrasonic treatment. *Journal of the Science of Food and Agriculture, 100*(5), 2065–2073.

Ismaya, W. T., Rozeboom, H. J., Weijn, A., Mes, J. J., Fusetti, F., Wichers, H. J., & Dijkstra, B. W. (2011). Crystal structure of *Agaricus bisporus* mushroom tyrosinase: Identity of the tetramer subunits and interaction with tropolone. *Biochemistry, 50*(24), 5477–5486.

Jia, J., Gao, X., Hao, M., & Tang, L. (2017). Comparison of binding interaction between β-lactoglobulin and three common polyphenols using multi-spectroscopy and modeling methods. *Food Chemistry, 228*, 143–151.

Jia, G. L., Shi, J. Y., Song, Z. H., & Li, F. D. (2015). Prevention of enzymatic browning of Chinese yam (*dioscorea spp.*) using electrolyzed oxidizing water. *Journal of Food Science, 80*, 718–728.

Li, X., Bai, Y., Ji, H., & Jin, Z. (2020). The binding mechanism between cyclodextrins and pullulanase - A molecular docking, isothermal titration calorimetry, circular dichroism and fluorescence study. *Food Chemistry, 321*, Article 126750.

Liao, T., Zhou, L., Liu, J., Zou, L., Dai, T., & Liu, W. (2021). Inhibitory mechanism of salicylic acid on polyphenol oxidase: A cooperation between acidification and binding effects. *Food Chemistry, 348*, Article 129100.

Marusek, C. M., Trobaugh, N. M., Flurkey, W. H., & Inlow, J. K. (2006). Comparative analysis of polyphenol oxidase from plant and fungal species. *Journal of Inorganic Biochemistry., 100*, 108–123.

Micsonai, A., Wien, F., Bulyáki, É., Kun, J., Moussong, É., Lee, Y. H., … Kardos, J. (2018). BeStSel: A web server for accurate protein secondary structure prediction and fold recognition from the circular dichroism spectra. *Nucleic Acids Research, 46*(1), 315–322.

Nirmal, N. P., & Benjakul, S. (2012). Inhibition kinetics of catechin and ferulic acid on polyphenoloxidase from cephalothorax of Pacific white shrimp (*Litopenaeus vannamei*). *Food Chemistry, 131*(2), 569–573.

Nirmal, N. P., Benjakul, S., Ahmad, M., Arfat, Y. A., & Panichayupakaranant, P. (2015). Undesirable enzymatic browning in crustaceans: Causative effects and its inhibition by phenolic compounds. *Critical Reviews in Food Science and Nutrition, 55*(14), 1992–2003.

Rahman, S., Khan, I., & Oh, D. H. (2016). Electrolyzed water as a novel sanitizer in the food industry: Current trends and future perspectives. *Comprehensive Reviews in Food Science and Food Safety, 15*, 1–20.

Ramsay, R. R., & Tipton, K. F. (2017). Assessment of enzyme inhibition: A review with examples from the development of monoamine oxidase and cholinesterase inhibitory drugs. *Molecules, 22*(7), 1192.

Ran, X., Yang, Z., Chen, Y., & Yang, H. (2022). Konjac glucomannan decreases metabolite release of a plant-based fishball analogue during *in vitro* digestion by affecting amino acid and carbohydrate metabolic pathways. *Food Hydrocolloids, 129*, Article 107623.

Ren, C., Xiong, W., Li, J., & Li, B. (2019). Comparison of binding interactions of cyanidin-3-O-glucoside to β-conglycinin and glycinin using multi-spectroscopic and thermodynamic methods. *Food Hydrocolloids, 92*, 155–162.

Sabarre, D. C., Jr, & Yagonia-Lobarbio, C. F. (2022). Extraction and characterization of polyphenol oxidase from plant materials: A Review. *Journal of Applied Biotechnology Reports, 8*(2), 83–95.

Sae-leaw, T., & Benjakul, S. (2019). Prevention of melanosis in crustaceans by plant polyphenols - A review. *Trends in Food Science & Technology, 85*, 1–9.

Sae-leaw, T., Benjakul, S., & Simpson, B. K. (2017). Effect of catechin and its derivatives on inhibition of polyphenoloxidase and melanosis of Pacific white shrimp. *Journal of Food Science and Technology, 54*(5), 1098–1107.

Sugumaran, M., Evans, J., Ito, S., & Wakamatsu, K. (2020). Nonenzymatic spontaneous oxidative transformation of 5, 6-dihydroxyindole. *International Journal of Molecular Sciences, 21*(19), 7321.

Swarup, R., & Jong-Whan, R. (2021). New insight into melanin for food packaging and biotechnology applications. *Critical Reviews in Food Science and Nutrition*, 1–27.

Yang, W., Xu, C., Liu, F., Yuan, F., & Gao, Y. (2014). Native and thermally modified protein−polyphenol coassemblies: Lactoferrin-Based nanoparticles and submicrometer particles as protective vehicles for (−)-epigallocatechin-3-gallate. *Journal of Agricultural and Food Chemistry, 62*(44), 10816–10827.

Zhou, L., Liu, W., Xiong, Z., Zou, L., Liu, J., Zhong, J., & Chen, J. (2016). Effect of ultrasound combined with malic acid on the activity and conformation of mushroom (*Agaricus bisporus*) polyphenoloxidase. *Enzyme and Microbial Technology, 90*, 61–68.

Zhou, L., Xiong, Z., Liu, W., & Zou, L. (2017). Different inhibition mechanisms of gentisic acid and cyaniding-3-O-glucoside on polyphenoloxidase. *Food chemistry, 234*, 445–454.

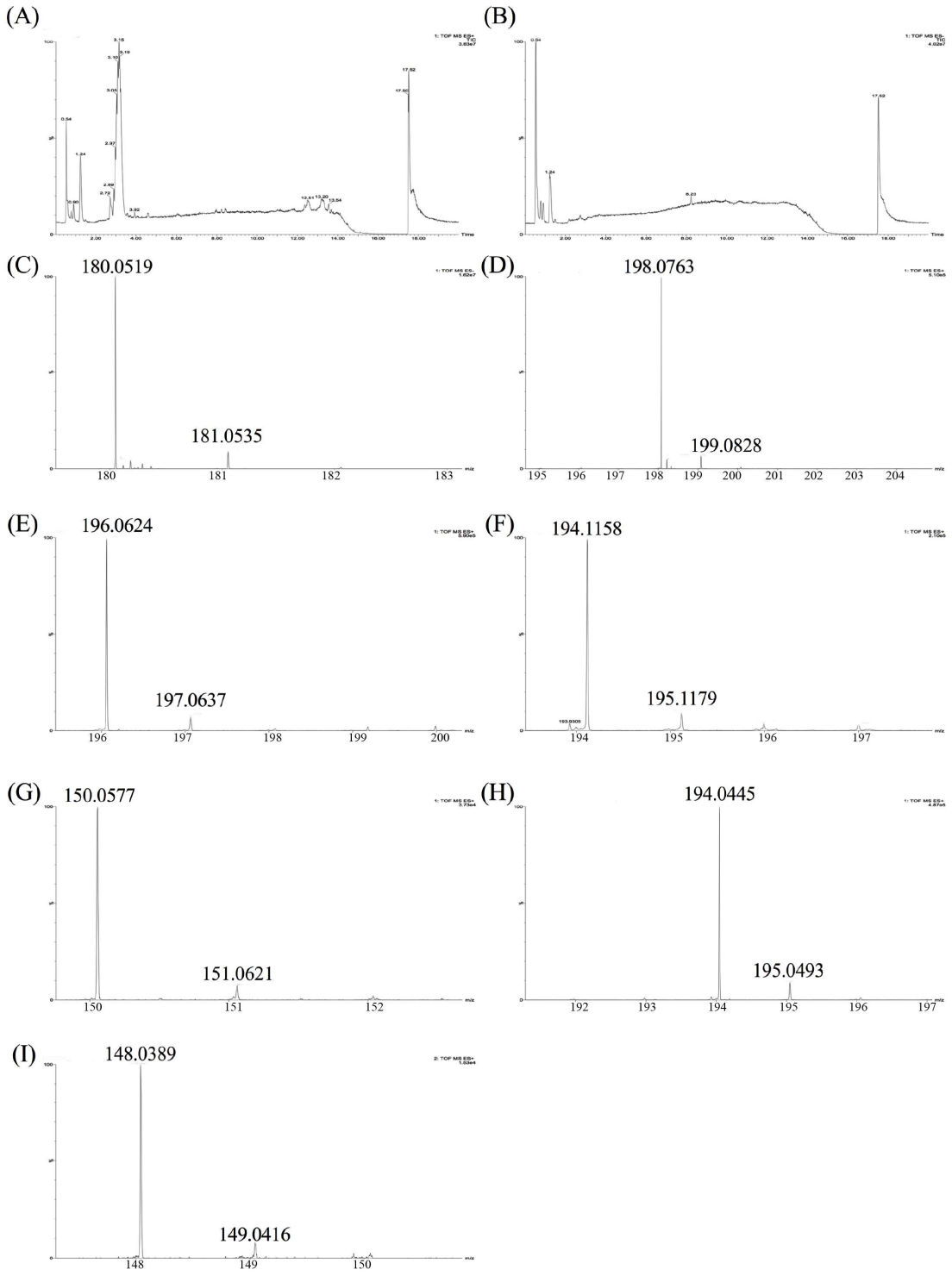

Fig. S1. Chromatograms of reaction products in positive ionization mode (A), negative ionisation mode (B), mass spectra of tyrosine (C), dihydroxyphenylalanine (DOPA) (D), Dopaquinone (E), Dopachrome (F), 5,6-dihydroxyindole (G), 5,6-dihydroxyindole-2-carboxylic acid (H), and 5,6-indolequinone (I).

Table S1. The overview of potential reaction products detected by UPLC-MS in different treated groups.

Putative identified compound	Product ions (m/z)	m/z	Retention time (min)	Score (out of 60)	Fragmentation Score	C/S		C/H		H/S	
						FC	*P* value	FC	*P* value	FC	*P* value
Tyrosine	$[M - H]^-$	180.0664	2.00	54.8	77.3	0.93	8.8E-03	0.96	2.5E-02	1.03	0.16
Dihydroxyphenylalanine (DOPA)	$[M + H]^+$	198.0766	1.01	46.7	52.9	9.20	2.6E-06	2.90	2.0E-03	3.17	6.3E-03
Dopaquinone	$[M + H]^+$	196.0605	1.23	49.3	47.5	3.57	3.9E-04	2.81	4.7E-06	1.27	0.24
Dopachrome	$[M + H]^+$	194.1150	3.26	51.2	62	2.74	4.5E-04	2.81	3.6E-06	1.23	0.23
5,6-dihydroxyindole	$[M + H]^+$	150.0551	1.23	49.2	48.7	3.47	2.6E-04	2.75	1.6E-06	1.26	0.22
5,6-dihydroxyindole-2-carboxylic acid	$[M + H]^+$	194.0451	2.57	49.9	55.6	5.03	4.1E-05	3.58	3.5E-07	1.40	0.09
5,6-indolequinone	$[M + H]^+$	148.0398	2.57	47.5	43.7	4.74	3.3E-04	3.39	1.2E-07	1.40	0.08

Note: C/S: Control group/SAEW group; C/H: Control group/ HOCl group; H/S: HOCl group/SAEW group; FC: fold change.